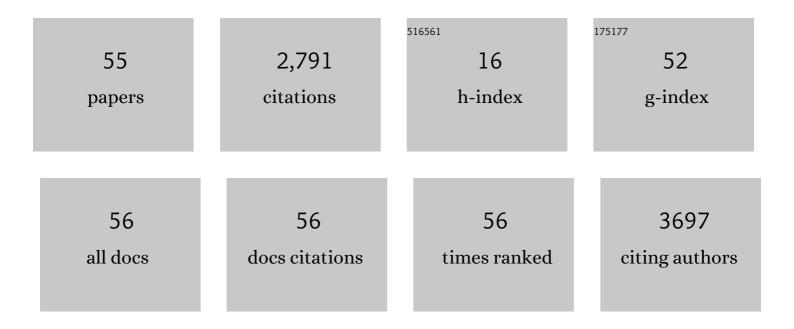
## Qihuang Deng

List of Publications by Year in descending order

Source: https://exaly.com/author-pdf/2190052/publications.pdf Version: 2024-02-01



OTHUANG DENG

#	Article	IF	CITATIONS
1	Conductive V2C MXene and paralelectric SrTiO3 containing polymer composites with high dielectric constant. Colloids and Surfaces A: Physicochemical and Engineering Aspects, 2022, 632, 127763.	2.3	11
2	Achieving a high dielectric constant and low dielectric loss of polymer composites filled with an interface-bonded g-C3N4@PbS narrow-bandgap semiconductor. Colloids and Surfaces A: Physicochemical and Engineering Aspects, 2022, 640, 128501.	2.3	3
3	Enhancing surface polarization and reducing bandgap of BaTiO3 nanofiller for preparing dielectric traits-improved composites via its hybridization with layered g-C3N4. Surfaces and Interfaces, 2022, 31, 102060.	1.5	5
4	Obtaining high dielectric constant and breakdown strength in composites with asymmetric MXene filler and highly insulative PVC matrix. Surfaces and Interfaces, 2022, 32, 102133.	1.5	3
5	Improving Dielectric Properties in Novel P(VDF-HFP)/V2AlC MAX/Montmorillonite Composite Films via Interfacial Electric-Leakage Depressing Strategy. Electronic Materials Letters, 2021, 17, 54-62.	1.0	4
6	Boron nitride nanosheet-induced low dielectric loss and conductivity in PVDF-based high-k ternary composites bearing ionic liquid. Materials Today Communications, 2021, 26, 101896.	0.9	11
7	Interfacial fluorine migration-induced low leakage conduction in PVA based high-k composites with V2C MXene-SWCNT switchboard-like ceramic via ab initio MD simulations. Journal of Materials Chemistry C, 2021, 9, 1051-1061.	2.7	11
8	Finely-reconciled high dielectric constant and low dielectric loss in ternary polymer/Cr2C3/montmorillonite composite films by filler-synergy strategy. Current Applied Physics, 2021, 22, 104-110.	1.1	11
9	Remarkably Elevated Permittivity Achieved in PVDF/1D La2TiO5 Composite Film Materials with Low-Level Dielectric Loss by Adding 2D V2C MXene Phase. Journal of Electronic Materials, 2021, 50, 2182-2189.	1.0	2
10	Improving electric insulation characteristics of PVA/V2C MXene composite high-dielectric-constant films by blending cellulose. Journal of the Australian Ceramic Society, 2021, 57, 819-824.	1.1	3
11	Remarkably improving dielectric response of polymer/hybrid ceramic composites based on 0D/2D-stacked CuO/V2C MXene heterojunction. Applied Surface Science, 2021, 545, 149008.	3.1	17
12	Reinforced dielectric response in polymer/V2C MXene composite high-insulation films enabled through dispersing ionic liquid. Journal of Electroceramics, 2021, 46, 124-130.	0.8	3
13	Enhanced dielectric response of ternary polymeric composite films via interfacial bonding between V2C MXene and wide-bandgap ZnS. Ceramics International, 2021, 47, 32938-32946.	2.3	9
14	Lowering Dielectric Loss and AC Conductivity of Polymer/HfC Composite Dielectric Films via Insulating Montmorillonite Barrier. Macromolecular Research, 2021, 29, 589-596.	1.0	5
15	Preparation of hybrid ceramic/PVC composites showing both high dielectric constant and breakdown strength ascribed to interfacial effect between V2C MXene and Cu2O. Colloids and Surfaces A: Physicochemical and Engineering Aspects, 2021, 630, 127650.	2.3	13
16	Enabling high dielectric response and low electrical leakage in polymer/mesoporous-silica@CdTe-quantum-dots nanocomposites by excitonic dipoles and pore-canal restriction. Ceramics International, 2021, 47, 26829-26838.	2.3	4
17	Well-coordinated dielectric properties in polymer composites bearing hybrid ceramic via interfacial effect between Ti2C MXene particles and large-aspect-ratio ZrO2 fibers. Colloids and Surfaces A: Physicochemical and Engineering Aspects, 2021, 629, 127505.	2.3	5
18	Solvothermal synthesis of in situ nitrogen-doped Ti3C2 MXene fluorescent quantum dots for selective Cu2+ detection. Ceramics International, 2020, 46, 8320-8327.	2.3	90

QIHUANG DENG

#	Article	IF	CITATIONS
19	Well-balanced high permittivity and low dielectric loss obtained in PVDF/graphite/BN ternary composites by depressing interfacial leakage conduction. Microelectronic Engineering, 2020, 231, 111404.	1.1	8
20	Interface Enhancement-Induced Improvement of Dielectric Traits in Poly(Ether Sulfone)/Ti3C2 MXene/KH550 Nanocomposites. Journal of Electronic Materials, 2020, 49, 7547-7559.	1.0	5
21	Enabling High Dielectric Response in PVDF/V <sub>2</sub> C MXene–TiO <sub>2</sub> Composites Based on Nontypical V–F–Ti Bonding and Fermi-Level Overlapping Mechanisms. Journal of Physical Chemistry C, 2020, 124, 27780-27789.	1.5	17
22	Realizing Rationally-Balanced Dielectric Properties in Fluoropolymer/Cr2AlC MAX Composites Modified by 2D-BN. Macromolecular Research, 2020, 28, 1261-1267.	1.0	4
23	Eco-friendly poly(vinyl alcohol)/delaminated V2C MXene high-k nanocomposites with low dielectric loss enabled by moderate polarization and charge density at the interface. Ceramics International, 2020, 46, 27326-27335.	2.3	17
24	Boro/carbothermal reduction synthesis of uranium tetraboride and its oxidation behavior in dry air. Journal of the American Ceramic Society, 2019, 102, 1049-1056.	1.9	4
25	Effect of La-doped scheelite-type SrWO4 for photocatalytic H2 production. Ionics, 2019, 25, 5083-5089.	1.2	7
26	A rational design for reconciling high permittivity and breakdown strength in layered PVDF composites from TaB <sub>2</sub> @Ta <sub>2</sub> O <sub>5</sub> nanofiller induced Schottky barrier effect. Journal of Materials Chemistry C, 2019, 7, 9975-9983.	2.7	4
27	Mediating dielectric/breakdown conflict in polydopamine@HfB2 nanorod-filled polymer composites from rational meaty-sandwich structure. Journal of Materials Science: Materials in Electronics, 2019, 30, 21305-21315.	1.1	0
28	Three-dimensional interconnected Co(OH) <sub>2</sub> nanosheets on Ti mesh as a highly sensitive electrochemical sensor for hydrazine detection. New Journal of Chemistry, 2019, 43, 3218-3225.	1.4	32
29	High-energy density in Si-based layered nanoceramic/polymer composites based on gradient design of ceramic bandgaps. Ceramics International, 2019, 45, 16600-16607.	2.3	8
30	Three-dimensional flower-like Ni–Mn–S on Ti mesh: a monolithic electrochemical platform for detecting glucose. New Journal of Chemistry, 2019, 43, 7866-7873.	1.4	5
31	High dielectric and breakdown properties obtained in a PVDF based nanocomposite with sandwich structure at high temperature <i>via</i> all-2D design. Journal of Materials Chemistry C, 2019, 7, 6744-6751.	2.7	56
32	Strong interface effect induced high-k property in polymer based ternary composites filled with 2D layered Ti3C2 MXene nanosheets. Journal of Materials Science: Materials in Electronics, 2019, 30, 9106-9113.	1.1	8
33	Enhanced Hydrogen Evolution Activity of Ni/Ni <sub>3</sub> S <sub>2</sub> Nanosheet Grown on Ti Mesh by Cu Doped Ni. Journal of the Electrochemical Society, 2019, 166, F168-F173.	1.3	8
34	Study on gel weight fraction of ultraviolet-cured acrylic adhesives. Chemical Papers, 2019, 73, 517-524.	1.0	2
35	Highly Retained Electric and Mechanical Traits in Micron-Sized Glass Fibers Filled Epoxy Composite Based on Heat-Oxygen Ageing. Journal of Inorganic and Organometallic Polymers and Materials, 2019, 29, 66-71.	1.9	3
36	High dielectric and breakdown properties achieved in ternary BaTiO3/MXene/PVDF nanocomposites with low-concentration fillers from enhanced interface polarization. Ceramics International, 2019, 45, 7923-7930.	2.3	86

QIHUANG DENG

#	Article	IF	CITATIONS
37	Superhydrophobic nanocomposite coatings with photoinitiated three-dimensional networks based on reactive graphene nanosheet-induced self-wrinkling patterned surfaces. Journal of Colloid and Interface Science, 2019, 536, 149-159.	5.0	7
38	Finely depressed dielectric loss and conductivity achieved in high-kappa stannic oxide/polymer nanocomposites from surfactant-assisted electric percolation. Journal of Materials Science: Materials in Electronics, 2019, 30, 2682-2692.	1.1	3
39	Synthesis and properties of conductive B <sub>4</sub> C ceramic composites with TiB <sub>2</sub> grain network. Journal of the American Ceramic Society, 2018, 101, 3780-3786.	1.9	38
40	Novel Scale‣ike Structures of Graphite/TiC/Ti <sub>3</sub> C <sub>2</sub> Hybrids for Electromagnetic Absorption. Advanced Electronic Materials, 2018, 4, 1700617.	2.6	86
41	Lowâ€temperature synthesis of uranium monocarbide by a Pechiniâ€type in situ polymerizable complex method. Journal of the American Ceramic Society, 2018, 101, 2786-2795.	1.9	0
42	Low temperature synthesis of TaB <sub>2</sub> nanorods by moltenâ€salt assisted borothermal reduction. Journal of the American Ceramic Society, 2018, 101, 45-49.	1.9	13
43	An ultrahigh discharged energy density achieved in an inhomogeneous PVDF dielectric composite filled with 2D MXene nanosheets <i>via</i> interface engineering. Journal of Materials Chemistry C, 2018, 6, 13283-13292.	2.7	71
44	Annealing and Stretching Induced High Energy Storage Properties in All-Organic Composite Dielectric Films. Materials, 2018, 11, 2279.	1.3	3
45	Ni Nanoparticle Anchored on MWCNT as a Novel Electrochemical Sensor for Detection of Phenol. Nano, 2018, 13, 1850134.	0.5	10
46	Photoluminescent Ti <sub>3</sub> C <sub>2</sub> MXene Quantum Dots for Multicolor Cellular Imaging. Advanced Materials, 2017, 29, 1604847.	11.1	692
47	Enhanced thermal properties of poly(vinylidene fluoride) composites with ultrathin nanosheets of MXene. RSC Advances, 2017, 7, 20494-20501.	1.7	242
48	Electrochemical corrosion behavior and surface modification of ZrB <sub>2</sub> in hydrofluoric acid aqueous solution. International Journal of Applied Ceramic Technology, 2017, 14, 779-784.	1.1	1
49	Facile preparation of in situ coated Ti <sub>3</sub> C <sub>2</sub> T <sub>x</sub> /Ni <sub>0.5</sub> Zn <sub>0.5</sub> Fe <sub>2</sub> O <sub>4 and their electromagnetic performance. RSC Advances, 2017, 7, 24698-24708.</sub>	cor	np <b>osit</b> es
50	Densification and mechanical properties of pulsed electric current sintered B4C with in situ synthesized Al3BC obtained by the molten-salt method. Journal of the European Ceramic Society, 2017, 37, 4524-4531.	2.8	25
51	Cytocompatibility of Ti <sub>3</sub> AlC <sub>2</sub> , Ti <sub>3</sub> SiC <sub>2</sub> , and Ti <sub>2</sub> AlN: <i>In Vitro</i> Tests and First-Principles Calculations. ACS Biomaterials Science and Engineering, 2017, 3, 2293-2301.	2.6	75
52	Highly Flexible, Freestanding Supercapacitor Electrode with Enhanced Performance Obtained by Hybridizing Polypyrrole Chains with MXene. Advanced Energy Materials, 2016, 6, 1600969.	10.2	580
53	Loading Actinides in Multilayered Structures for Nuclear Waste Treatment: The First Case Study of Uranium Capture with Vanadium Carbide MXene. ACS Applied Materials & Interfaces, 2016, 8, 16396-16403.	4.0	214
54	Electronic structures and mechanical properties of Al(111)/ZrB <sub>2</sub> (0001) heterojunctions from first-principles calculation. Molecular Physics, 2015, 113, 1794-1801.	0.8	21

#	Article	IF	CITATIONS
55	Synthesis of Hexagonal Columnar <scp><scp>ZrB</scp></scp> <sub>2</sub> Powders Through Dissolutionâ€Recrystallization Approach by Microwave Heating Method. Journal of the American Ceramic Society, 2014, 97, 3037-3040.	1.9	16